Second Harmonic Optical Activity of Tryptophan Derivatives Adsorbed at the Air/Water Interface

S. A. Mitchell* and R. A. McAloney

Steacie Institute for Molecular Sciences, National Research Council of Canada, 100 Sussex Drive, Ottawa, Ontario K1A 0R6, Canada

Received: August 1, 2003; In Final Form: November 6, 2003

Optical activity in second harmonic reflection from the air/water interface of solutions of simple tryptophan (trp) derivatives has been investigated. The derivatives include D- and L-optical isomers of Boc-trp and DD- and LL-isomers of the dipeptide Boc-trp-trp, where Boc is *tert*-butyloxycarbonyl. An experimental method based on polarization modulation of fundamental radiation by rotation of a quarter-wave retardation plate has been used to completely characterize the second-order nonlinear susceptibilities of the chiral surfaces, for the fundamental wavelength $\lambda = 564$ nm. Boc-trp and Boc-trp-trp show similar chiral contributions to the nonlinear susceptibilities, which indicates that the chiral response does not depend on intramolecular interactions between trp residues. The efficiency of second harmonic reflection has been shown to be resonantly enhanced at the two-photon level, in the region of the near-UV bands (∼280 nm) of the indole chromophore of tryptophan. The origin of the chiral response is discussed in terms of simple microscopic models, and a comparison is made with optical activity of tryptophanyl compounds in linear spectroscopy. The peptide gramicidin, incorporating several trp residues, showed no evidence of optical activity in second harmonic reflection from the air/water interface. This indicates that second harmonic optical activity is sensitive to structural effects such as conformational and orientational distributions of trp residues at the interface.

1. Introduction

Following the first reports of optical activity in second harmonic reflection from chiral surfaces in 1993−94,[1−7] there has been growing interest in the application of second harmonic generation optical activity (SHG-OA) for studies of biomolecules adsorbed at interfaces. SHG-OA measurements have the potential for providing unique information on conformations and conformational changes of surface-active biological molecules. Such a potential is anticipated by analogy with well-developed linear chiroptical measurements on biomolecules in bulk solution.[8] Second harmonic generation (SHG) is inherently sensitive to surfaces and interfaces.[9] Furthermore, the sensitivity of SHG-OA measurements is very high in comparison with linear chiroptical methods, potentially in the submonolayer range.[1]

There have been relatively few SHG studies of amino acid derivatives adsorbed at surfaces. Smiley and Vogel[10−12] studied aromatic amino acid derivatives at the air/water interface and used resonance enhanced SHG to probe interfacial tryptophan (trp) residues. Frey and co-workers[7] reported observations of SHG-OA for the dipeptide Boc-trp-trp adsorbed at the air/water interface (Boc represents a *tert*-butyloxycarbonyl protecting group). SHG-OA was observed for Boc-trp-trp when the second harmonic of the laser wavelength was resonant with the indole chromophore of tryptophan ($\lambda/2 \sim 280$ nm). SHG-OA has also been reported for supported films of bacteriorhodopsin,[5] for the protein cytochrome *c* at air/water interface,[13] and most recently for the peptide melittin bound to the surface of a planar-supported lipid bilayer.[14] Girault and co-workers[15] have used SHG to study the enzyme glucose oxidase adsorbed at air/water interface and also the heme proteins myoglobin and hemoglobin adsorbed at a liquid/liquid interface. Nonlinear optical studies of interfacial biomolecules have also been carried out using sum frequency generation vibrational spectroscopy.[16−18]

The theory of SHG-OA of chiral surfaces is well established at the phenomenological level,[19,20] and aspects of the microscopic origin of the nonlinear optical response have been studied.[21−27] At this time there is a need for experimental evidence on relevant microscopic mechanisms, and to establish correlations that can provide input for the development of useful descriptive models. In this work we have reinvestigated the Boc-trp-trp and Boc-trp systems originally studied by Frey and co-workers[7] and by Smiley and Vogel.[10−12] We have used recently developed measurement techniques[20,28−30] to provide a thorough characterization of SHG-OA of the trp systems. Our results provide new information on the origin of SHG-OA of tryptophan derivatives at the air/water interface.

2. Experimental Section

2.1. Laser System and Setup for SHG. A schematic diagram of the experimental setup for measurement of optical activity in second harmonic reflection from an air/water interface is shown in Figure 1. Tunable laser pulses from a femtosecond optical parametric oscillator (OPA) are incident on the interface at 60° from the surface normal. A Berek's compensator (BC) and Glan polarizer (GP) are used to initially select *p*-polarization of the laser radiation, which is incident on an achromatic quarter-wave retardation plate (AWP). Rotation of the AWP through 360° in a plane normal to the laser beam produces a well-defined modulation of the polarization state of the fundamental radiation, including left- and right-hand circular polarization states. Second harmonic radiation reflected from the air/water interface in the specular direction is resolved in selected plane-polarized states by using a Rochon prism polarizer (RP). The AWP and RP are

10.1021/jp036252e CCC: $27.50 Published 2004 by the American Chemical Society
Published on Web 12/18/2003

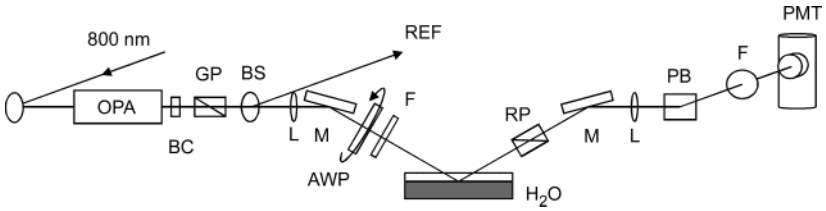

Figure 1. Schematic diagram of experimental setup for measurement of optical activity in second harmonic reflection from an air/water interface. Key: OPA, optical parametric amplifier; BC, Berek's polarization compensator; GP, Glan laser prism; BS, beam splitter; L, lens; M, mirror; AWP, achromatic wave plate; F, filter; RP, Rochon prism polarizer; PB, Pellin-Broca prism; PMT, photomultiplier tube. The PMT, setup for reference SHG signal (REF), and laser source for 800 nm pump radiation are behind the plane of incidence at the air/water interface.

mounted directly in the incident and reflected laser beams, respectively, at appropriate angles to the horizontal. Second harmonic and fundamental light reflected from the air/water interface are spatially separated by using a Pellin-Broca prism (PB). Colored glass filters (F) are used after the AWP to eliminate second harmonic radiation from the beam incident on the air/water interface and after the PB to selectively transmit second harmonic from the interface for detection on the photomultiplier tube (PMT).

In all experiments, a reference SHG signal from a quartz plate was measured simultaneously with the SHG signal from the sample. The reference signal was used to normalize the SHG signal for fluctuations in the incident laser power. In addition, the SHG measurements were normalized to a signal that was recorded when a z-cut quartz wedge was substituted in the sample position.

The OPA is a traveling-wave optical parametric amplifier of superfluorescence (Topas, Light Conversion). The Topas was pumped with the output of a 1 kHz Ti:sapphire regenerative amplifier (Positive light) seeded with the output of a femtosecond Ti:sapphire oscillator (Spectra-physics). Visible laser pulses in the range 500−600 nm and with a duration of ∼100 fs were produced by the OPA with a repetition rate of 1 kHz. Laser pulses with energy ∼2.0 μJ/pulse were focused on the air/water interface by using a 30 cm length focal lens. The beam waist at the focus had a diameter ∼140 μm, measured by translating a knife edge across the beam waist while monitoring the transmitted energy on a photodiode. The Berek's polarization compensator was obtained from New Focus, and the calcite Glan-laser polarizer, from Newport. The achromatic wave plate, with approximately quarter-wave retardance in the range 500−800 nm, was supplied by Halbo Optics. The magnesium fluoride Rochon polarizer was supplied by Karl Lambrecht, and the Pellin-Broca prism, by B. Halle Nachfl. (Berlin).

The sample cell is an open dish fabricated from Teflon, with a well diameter 7.2 cm and depth 1.7 cm. It was filled with 40 mL of sample solution. The large diameter of the cell provided a flat fluid surface for undistorted reflection of the laser beam. The second harmonic signal was detected with a solar-blind photomultiplier tube (Hamamatsu) and averaged by using a gated integrator (Stanford Research Systems). Typically, 1000−3000 pulses were averaged for each point of a wave plate rotation trace. It was confirmed that the second harmonic signal varied quadratically with the pulse energy of the fundamental radiation. Repeated measurements on the same samples showed no indication of laser induced degradation of the samples during data acquisition.

2.2. Materials and Sample Preparation. N_α-(*tert*-butoxycarbonyl)-L-tryptophan (L-trp) from Aldrich, N_α-(*tert*-butoxycarbonyl)-D-tryptophan (D-trp) from Flulka, and 2,7-dihydroxynaphthalene (DHN) from Aldrich were used as received. Citrate buffer was prepared from citric acid monohydrate (EM Science) and sodium citrate dihydrate (Aldrich). All solutions were prepared using Milli-Q water (resistivity > 18 MΩ cm).

Gramicidin D (gD) from Sigma is a linear polypeptide complex consisting of gramicidin types A−C. The major component is gramicidin A, with the sequence formyl-L-Val-Gly-L-Ala-D-Leu-L-Ala-D-Val-L-Val-D-Val-L-Trp-D-Leu-L-Trp-D-Leu-L-Trp-D-Leu-L-Trp-ethanolamine. A solution of gD in methanol (1 mg/mL) was mixed with a solution of the lipid 1,2-dipalmitoyl-*sn*-glycero-3-phosphocholine (DPPC) in $CHCl_3$ (1 mg/mL). The DPPC/gD mixture (50% mole ratio) was used to prepare a layer at the air/water interface by dropping a few microliters on the surface. This preparation resulted in a homogeneous film with a surface pressure ∼25 mN/m. Solutions of DHN were saturated solutions in water, carefully decanted, and then filtered with a 450 μm Millipore filter.

Synthesis of Boc-(L)Trp-(L)Trp and Boc-(D)Trp-(D)Trp. The Boc-protected L-tryptophan amino acid was coupled to the corresponding methyl ester protected L-tryptophan with 1,3-diisopropylcarbodiimide in the presence of *N*,*N*-diisopropylethylamine and 1-hydroxybenzotriazole in freshly distilled dichloromethane. After purification by column chromatography, the methyl ester was hydrolyzed to the free acid by treating with sodium hydroxide in a water/DMF mixture. The reaction is shown in Scheme 1. Neutralization and extraction with dichloromethane yielded the Boc-protected LL-tryptophan dipeptide (LL-trp) in a 95% overall yield. The Boc-protected DD-tryptophan dipeptide (DD-trp) was synthesized in the same manner.

We shall refer to L-trp (D-trp) and LL-trp (DD-trp) as Boc-trp and Boc-trp-trp, respectively, when the enantiomeric form is not important.

Solutions of the tryptophan compounds were prepared in 22 mM citrate buffer with pH in the range 3.3−3.4. Boc-trp solid was dissolved in a solution of sodium citrate dihydrate using a minimal amount of water (∼10 mL). Dissolution occurred after 10−15 min of sonication. Once dissolved, the citrate/trp solution was slowly combined with the citric acid solution and diluted to 1.0 mM in Boc-trp. The dipeptide solutions were prepared using the same procedure, to 0.1 mM Boc-trp-trp and 22 mM citrate buffer. The sample solutions were characterized by using high-performance liquid chromatography, which confirmed that only single tryptophan species were present, i.e., Boc-trp or Boc-trp-trp. Circular dichroism (CD) spectroscopy (Jasco J-600 spectropolarimeter) was used to confirm the enantiomeric purity of the materials. Distinct CD spectra were observed for the Boc-trp and Boc-trp-trp solutions in the region 240−320 nm.

3. Results and Analysis

3.1. Second Harmonic Generation. Smiley and Vogel[10] have studied adsorption of Boc-trp at the air/water interface of a bulk solution of Boc-trp in a citrate buffer with pH 3.2. Surface pressure and SHG measurements indicated a well-defined

SCHEME 1

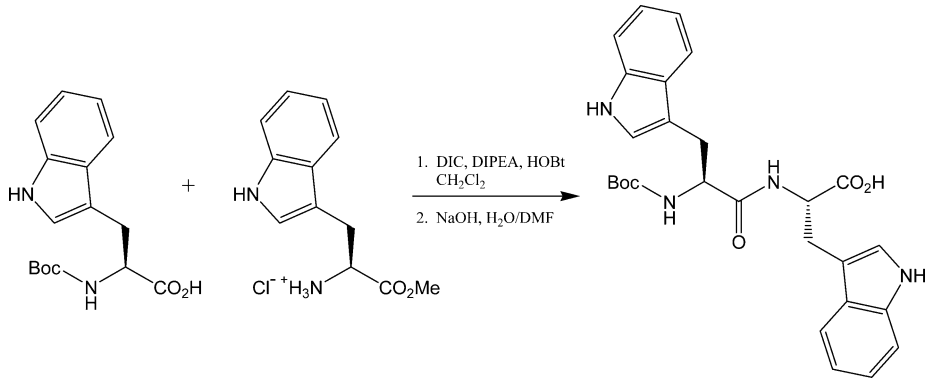

adsorption behavior with increasing bulk concentration. A monolayer film with a surface density of Boc-trp ~1.7 nm^{-2} was formed for a bulk concentration of Boc-trp ~1 mM. We have repeated the surface pressure and SHG measurements of Smiley and Vogel and found general agreement. Similar measurements on Boc-trp-trp indicated significantly higher surface activity compared with Boc-trp. This was seen in the results of surface pressure measurements and also from observations of SHG signals from the air/solution interface.

The efficiency of second harmonic reflection R_{pp} for *p*-polarized fundamental and second harmonic radiation is defined in terms of the associated irradiances as shown in eq 1.

$$R_{pp} = \frac{I_p(2\omega)}{[I_p(\omega)]^2} \tag{1}$$

We measured R_{pp} for L-trp and gD adsorbed at air/water interface by calibrating the second harmonic response with the signal observed when a z-cut quartz crystal was substituted in the sample position. We used $d_{11} = 0.34$ pm/V for quartz with the fundamental wavelength $\lambda = 564$ nm, based on literature data[31] for $\lambda = 1064$ nm and application of Miller's rule to estimate the wavelength dependence of d_{11}. Measurements of R_{pp} for L-trp and gD were repeated for several fundamental wavelengths in the range $\lambda = 500-605$ nm, and the results are shown in Figure 2. Also shown in Figure 2 is an absorption spectrum of a bulk solution of L-trp in the citrate buffer. To facilitate comparison with the absorption spectrum, the wavelength scale for R_{pp} in Figure 2 is shown as the second harmonic wavelength, i.e., $\lambda/2$. We also show in Figure 2 the SHG efficiency measured for the aqueous buffer that was used to prepare the L-trp solutions, for the fundamental wavelength $\lambda = 564$ nm. The efficiency of second harmonic reflection from the L-trp solution exceeded that from the buffer with no L-trp by a factor ~10.

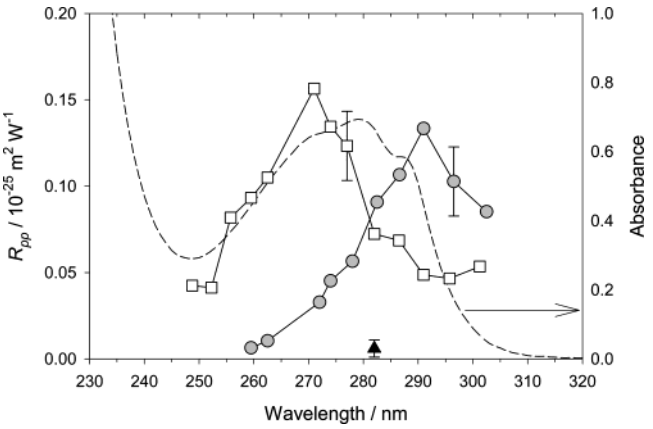

Figure 2. Spectra of second harmonic efficiency R_{pp} of L-trp (filled circles) and gD (open squares) at air/water interface, in comparison with absorption spectrum of L-trp in aqueous buffer solution (broken line). The wavelength scale for R_{pp} corresponds with the second harmonic of the fundamental wavelength ($\lambda/2$). The solid triangle shows R_{pp} for the buffer solution with no added L-trp, for $\lambda = 564$ nm. Error bars show representative uncertainties in relative values.

3.2. Second Harmonic Optical Activity. A detailed phenomenological theory of second harmonic optical activity (SHG-OA) of chiral surfaces including electric-dipole and higher order interactions has been presented by Maki et al.,[19] and a general approach for measurement and characterization of SHG-OA has been developed.[28−30] Here we outline some essential features for the particular case where only electric-dipole interactions are considered. Attention is restricted to isotropic surfaces with full rotational symmetry about the surface normal. A general expression for the intensity of reflected second harmonic radiation is given by eq 2, where $E_p(\omega)$ and $E_s(\omega)$ are complex valued amplitudes of *p*- and *s*-polarized components of the fundamental electric field (with angular frequency ω) incident on the nonlinear surface and *f*, *g*, and *h* are complex valued coefficients that are interpreted as effective nonlinear susceptibilities of the surface.

$$I_{2\omega} = |fE_p^2(\omega) + gE_s^2(\omega) + hE_p(\omega)E_s(\omega)|^2 \tag{2}$$

Maki et al.[19] have shown how the effective susceptibilities are related to more general nonlinear susceptibility tensors. In eq 2, particular values of the coefficients *f*, *g*, and *h* are associated with specific polarization states of the second harmonic radiation. For *p*-polarized second harmonic we designate the coefficients as f_p, g_p, and h_p, while f_s, g_s, and h_s are used for *s*-polarized second harmonic radiation. Additional subscripts 1 and 2 are used to indicate the real and imaginary parts of the coefficients, respectively: $f_p = f_{p1} + if_{p2}$, and similarly for g_p, h_p, f_s, g_s, and h_s. With the restriction to electric-dipole interactions and isotropic surfaces, the effective susceptibilities have the following properties: $g_s = 0$; $h_p \propto f_s \propto \chi^{(2)}_{XYZ}$, where $\chi^{(2)}_{XYZ}$ is the element of the nonlinear susceptibility tensor that is nonzero only for chiral surfaces. The chiral susceptibilities f_s and h_p are not independent; they are related by a multiplicative factor that depends on geometrical factors and optical constants of the interface. There are thus eight independent, real valued constants that completely specify the nonlinear response: f_{p1}, f_{p2}, g_{p1}, g_{p2}, h_{p1}, h_{p2}, h_{s1}, and h_{s2}. Considering that the overall phase of the response is not significant, this number is reduced to seven by setting $h_{s2} = 0$ and $h_{s1} > 0$. Of these seven, only h_{p1} and h_{p2} are specifically associated with the chiral response; i.e., they are nonzero only for chiral surfaces. The remaining five constants are in general nonzero for both chiral and achiral isotropic surfaces.

TABLE 1: Second-Order Nonlinear Susceptibilities for DHN and Several Tryptophan Derivatives Adsorbed at the Air/Water Interface, from Global Fits of Quarter-Wave Plate Rotation Data for $\lambda = 564$ nm[a]

susceptibility	DHN	D-trp	L-trp	DD-trp	LL-trp
f_p	0.067 − 1.1i	−0.69 + 0.54i	−0.64 + 0.60i	−0.66 + 0.25i	−0.70 + 0.36i
g_p	−0.075 − 1.0i	−0.28 + 0.44i	−0.54 + 0.73i	−0.21 + 0.50i	−0.75 + 0.81i
f_s	0.0	−0.021 − 0.032i	−0.020 + 0.091i	0.010 − 0.052i	−0.048 + 0.062i
h_s	0.56	0.97	1.0	1.1	1.1
χ_{ZZZ}	2.6 − 2.3i	0.95 + 1.7i	2.7 + 0.84i	1.9 − 0.63i	4.0 − 1.2i
χ_{ZXX}	−0.59 − 8.1i	−2.7 + 4.4i	−5.4 + 7.3i	−2.6 + 6.1i	−8.3 + 8.9i
χ_{XXZ}	2.3	5.1	5.4	7.3	6.5
χ_{XYZ}	0.0	−0.14 − 0.21i	−0.13 + 0.59i	0.08 − 0.41i	−0.34 + 0.44i

[a] Effective susceptibilities f_p, g_p, f_s, and h_s are given in arbitrary units, with a common normalization factor. Elements of the nonlinear susceptibility tensor χ_{IJK} are absolute values in units of 10^{-22} m^2 V^{-1}. The phases of the susceptibilities are relative values, with h_s constrained as real and positive. See the text for details.

Geiger et al.[28] and Maki et al.[30] have described the use of a quarter-wave retardation plate for single-valued determination of second-order nonlinear susceptibilities of surfaces with in-plane isotropy. The method involves rotation of the quarter-wave plate to modulate the polarization state of the fundamental radiation incident on the nonlinear surface. Using the analysis and conventions of Maki et al.,[30] the intensity of reflected second harmonic radiation can be expressed as shown in eq 3.

$$I_{2\omega} = (f_1^2 + f_2^2)[(A^2 + B^2)^2] + (g_1^2 + g_2^2)[(C^2 + D^2)^2] + (h_1^2 + h_2^2)[(A^2 + B^2)(C^2 + D^2)] + 2(f_1g_1 + f_2g_2)[(A^2 - B^2)(C^2 - D^2) + 4ABCD] + 2(f_1h_1 + f_2h_2)[(A^2 + B^2)(AC + BD)] + 4(f_1g_2 - f_2g_1)[(C^2 - D^2)AB - (A^2 - B^2)CD] + 2(f_1h_2 - f_2h_1)[(A^2 + B^2)(BC - AD)] + 2(g_1h_1 + g_2h_2)[(C^2 + D^2)(AC + BD)] + 2(g_1h_2 - g_2h_1)[(C^2 + D^2)(AD - BC)] \quad (3)$$

The quantities $A-D$ specify the *p*- and *s*-polarized components of the fundamental electric field (E_p and E_s) incident on the nonlinear surface. In the case where the fundamental radiation incident on the wave plate is *p*-polarized with complex amplitude E_p^0 (and with $E_s^0 = 0$), then $E_p = E_p^0$ $(A + iB)$ and $E_s = E_p^0(C + iD)$, where $A-D$ are given in eqs 4.

$$A = \cos(\delta); \quad B = -\sin(\delta)\cos(2\theta); \quad C = 0; \quad D = -\sin(\delta)\sin(2\theta) \quad (4)$$

Here δ is the linear retardation of the wave plate ($\delta = \pi/4$ for a quarter-wave plate) and θ is the angle between the fast axis of the wave plate and the unit vector for *p*-polarized light (with respect to the nonlinear surface). Right- and left-hand circularly polarized states of the fundamental radiation are produced for $\theta = \pi/4$ and $\theta = -\pi/4$, respectively.

The effective susceptibilities in eq 3 are f_p, g_p, and h_p for *p*-polarized second harmonic and f_s, g_s, and h_s for *s*-polarized second harmonic radiation. These quantities can be measured by making a nonlinear fit of $I_{2\omega}$ vs quarter-wave plate rotation angle θ (for the selected polarization state), according to eq 3. Such $I_{2\omega}(\theta)$ traces show characteristic features that allow quick identification of a possible chiral contribution to the nonlinear response. A nonzero chiral susceptibility h_p (or f_s) is immediately apparent in producing an asymmetry of the $I_{2\omega}(\theta)$ trace about the midpoint $\theta = 180°$ of the range $\theta = 0-360°$ of wave plate rotation, for both *p*- and *s*-polarized second harmonic detection.

As shown by Geiger et al.,[28] it is useful to measure $I_{2\omega}(\theta)$ traces for q_{45}- and q_{135}- as well as *s*- and *p*-polarization states of second harmonic radiation. Here q_{45} and q_{135} refer to plane-polarized states with the plane rotated 45 and 135°, respectively, from the *p*-direction. The complex amplitudes of the electric field of the second harmonic radiation are $E_{q(45)} = (E_s + E_p)/\sqrt{2}$ and $E_{q(135)} = (E_s - E_p)/\sqrt{2}$. Likewise, the effective susceptibilities are $f_{q(45)} = (f_s + f_p)/\sqrt{2}$ and $f_{q(135)} = (f_s - f_p)/\sqrt{2}$ and similarly for $g_{q(45)}$, $g_{q(135)}$ and $h_{q(45)}$, $h_{q(135)}$. Traces of $I_{2\omega}(\theta)$ for q_{45}-, q_{135}-, *s*-, and *p*-polarization states each provide unique information on the effective susceptibilities f_p, g_p, h_p, and h_s. Therefore, it is useful to simultaneously fit all four traces with a unique set of susceptibilities (global fit). As noted above, seven parameters are needed to describe the second-order nonlinear response of an isotropic chiral surface. The work of Geiger et al.[28] and Maki et al.[30] has shown that a unique determination of all seven parameters can be made by means of quarter-wave plate rotation measurements.

3.3. Nonlinear Susceptibilities Measured by Achromatic Wave Plate Rotation. An achromatic quarter-wave plate was used to measure the susceptibilities of DHN, D-trp, L-trp, DD-trp, and LL-trp at air/water interface, with the fundamental wavelength $\lambda = 564$ nm. For each system, four $I_{2\omega}(\theta)$ traces were recorded by selecting *s*-, *p*-, q_{45}-, and q_{135}-polarization states of the second harmonic. Hereafter we shall refer to these traces as *s*-out, *p*-out, etc. The four traces were simultaneously fit with seven parameters as described in section 3.2 (global fit). Optimization was by minimizing the sum of the squares of the deviations between calculated and observed ($I_{2\omega}$, θ) pairs according to eq 3. Suitable Fresnel factors were included on the right-hand side of eq 3 to account for the polarization dependence of the transmission efficiency of the Pellin-Broca prism. In Figures 3−5 we show measured and fitted $I_{2\omega}(\theta)$ traces for DHN, D-trp, and L-trp. Similar results were obtained for DD-trp and LL-trp. The agreement between measured and fitted $I_{2\omega}(\theta)$ traces was in all cases satisfactory. The parameters obtained from the global fits are summarized in Table 1.

DHN was included in this study as an example of an achiral system. Our results are indeed consistent with a vanishing chiral response for DHN. Thus, the susceptibility h_p was constrained as zero in the fit for DHN, and this produced a satisfactory result (Figure 3). However, certain features of the data for DHN seemed at first to indicate the presence of a small chiral response. In particular, there is a small asymmetry about $\theta = 180°$ in the *p*-out $I_{2\omega}(\theta)$ trace, noticeable for example at $\theta = 135$ and 225° in Figure 3. The origin of this apparent chiral response was traced to an artifact of the achromatic wave plate. This was proven by rotating the wave plate 180° about its fast axis, so the laser beam was incident on the opposite face of the plate. The effect was to reverse the sign of the apparent chiral response, such that the asymmetry about $\theta = 180°$ in the *p*-out $I_{2\omega}(\theta)$ trace was reversed. This artifact can be attributed to a

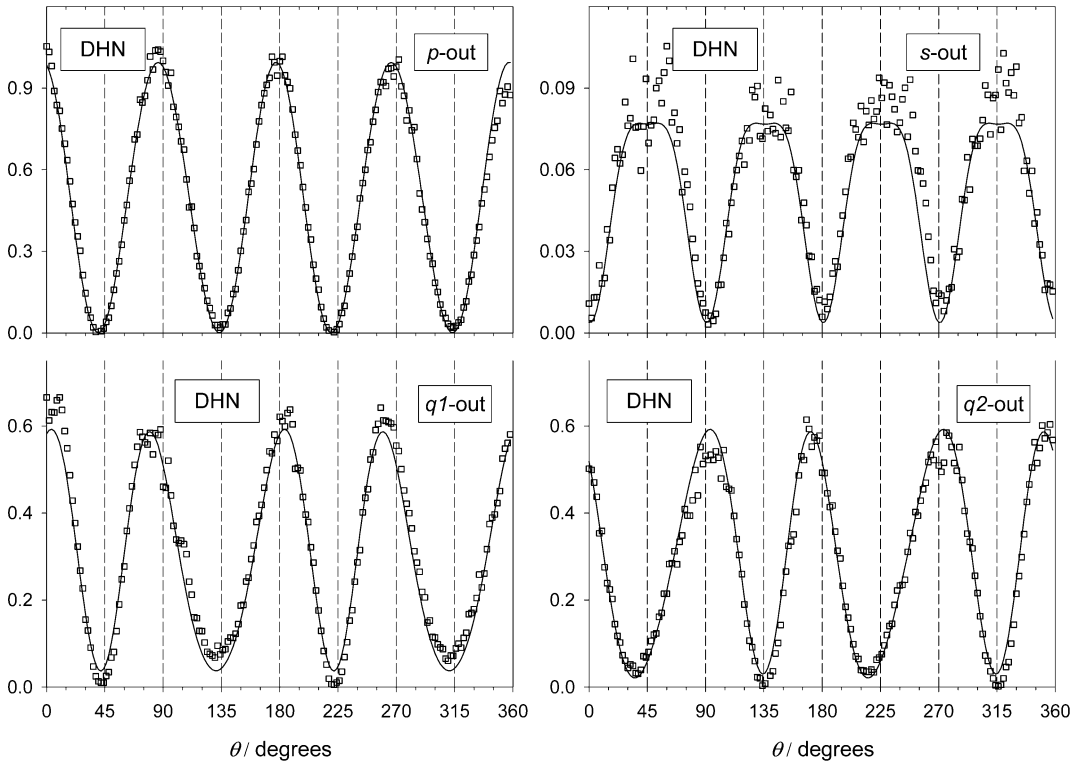

Figure 3. Global fits of wave plate rotation data $I_{2\omega}(\theta)$ for DHN at the air/water interface, for the indicated polarization states of second harmonic radiation. ($q1$ and $q2$ represent q_{45} and q_{135} polarization states, respectively.) The wavelength of fundamental radiation was $\lambda = 564$ nm. The second harmonic intensity is shown in the same arbitrary units in all traces.

misalignment of the two parallel retardation plates (quartz and magnesium fluoride) that comprise the achromatic retarder. Ideally, the fast axis of one plate should be aligned with the slow axis of the second plate. A misalignment of these axes about the normal to the plates introduces chirality in the setup, since the mirror plane defined by the normal to the plates and the optic axis is removed by such a misalignment.

We characterized the achromatic wave plate by recording θ-rotation traces $I_\omega(\theta)$ of the intensity of fundamental radiation transmitted by the wave plate in *s*-, *p*-, q_{45}- and q_{135}-polarization states, with *p*-polarized radiation incident on the wave plate. Here the polarization states are identical with those defined in section 3.2. The data were fit with four parameters that specify the details of the model of misaligned retardation plates: $\Delta\theta$ is the angle between the fast and slow axes of the two plates, δ' (δ) is the linear retardation of the magnesium fluoride (quartz) plate, and θ_0 gives the offset between the experimental variable θ_{obs} corresponding to the angular setting of the wave plate and the angle θ' between the fast axis of the magnesium fluoride retardation plate and the *p*-polarization direction. Additional quantities that depend on these parameters are defined in eqs 5−7.

$$\theta_{obs} = \theta' - \theta_0 \tag{5}$$

$$\theta = \theta' - \pi/2 + \Delta\theta \tag{6}$$

$$\delta = \delta' - \pi/4 + \Delta\delta \tag{7}$$

θ is the angle between the fast axis of the quartz retardation plate and the *p*-polarization direction. With this model the *s*- and *p*-polarized components of the transmitted electric field are $E_p = E_p^0(A + iB)$ and $E_s = E_p^0(C + iD)$, where E_p^0 is the amplitude of the *p*-polarized radiation incident on the wave plate and the quantities $A-D$ are given in eqns 8−11.

$$A = \cos(\delta')\cos(\delta) + \sin(\delta')\sin(\delta)\cos(2\Delta\theta) \tag{8}$$

$$B = -\cos(\delta')\sin(\delta)\cos(2\theta) - \sin(\delta')\cos(\delta)\cos(2\theta') \tag{9}$$

$$C = -\sin(\delta)\sin(\delta')\sin(2\Delta\theta) \tag{10}$$

$$D = -\sin(\delta')\cos(\delta)\sin(2\theta') - \sin(\delta)\cos(\delta')\sin(2\theta) \tag{11}$$

The amplitudes of the electric fields for q_{45}- and q_{135}-polarization states are related to E_p and E_s as described in section 3.2. Intensities of the transmitted radiation in the various polarization states are proportional to the absolute squares of the corresponding electric field amplitudes. Note that eqs 8−11 become equivalent to eqs 4 when the misalignment $\Delta\theta$ goes to zero.

Measured traces of $I_\omega(\theta)$ for *s*-, *p*-, q_{45}-, and q_{135}-polarization states were simultaneously fit with four parameters ($\Delta\theta$, δ', $\Delta\delta$, and θ_0), in the manner described above for $I_{2\omega}(\theta)$ traces (global fit). The fits to the data were excellent and yielded optimized parameters (all in angular units of deg): $\Delta\theta = 5$, $\delta' = 85.7$, $\Delta\delta = -1$, and $\theta_0 = 5$, for $\lambda = 564$ nm. Although this set of parameters is not unique, it nevertheless allows a useful correction to be applied in the analysis of the $I_{2\omega}(\theta)$ data. A careful investigation showed that it was unlikely that the nonunique nature of the correction introduced significant errors in the analysis. The correction is intended to compensate for the small chiral artifact introduced in the data by the misalignment of the elements of the achromatic wave plate. We applied this correction by using eqs 8−11 in place of eqs 4 to calculate the quantities $A-D$ in eq 3. The parameters in eqs 8−11 were fixed as given above; i.e., no additional free parameters were introduced. Including this correction in the fits produced markedly better results, as was apparent by eye and also from

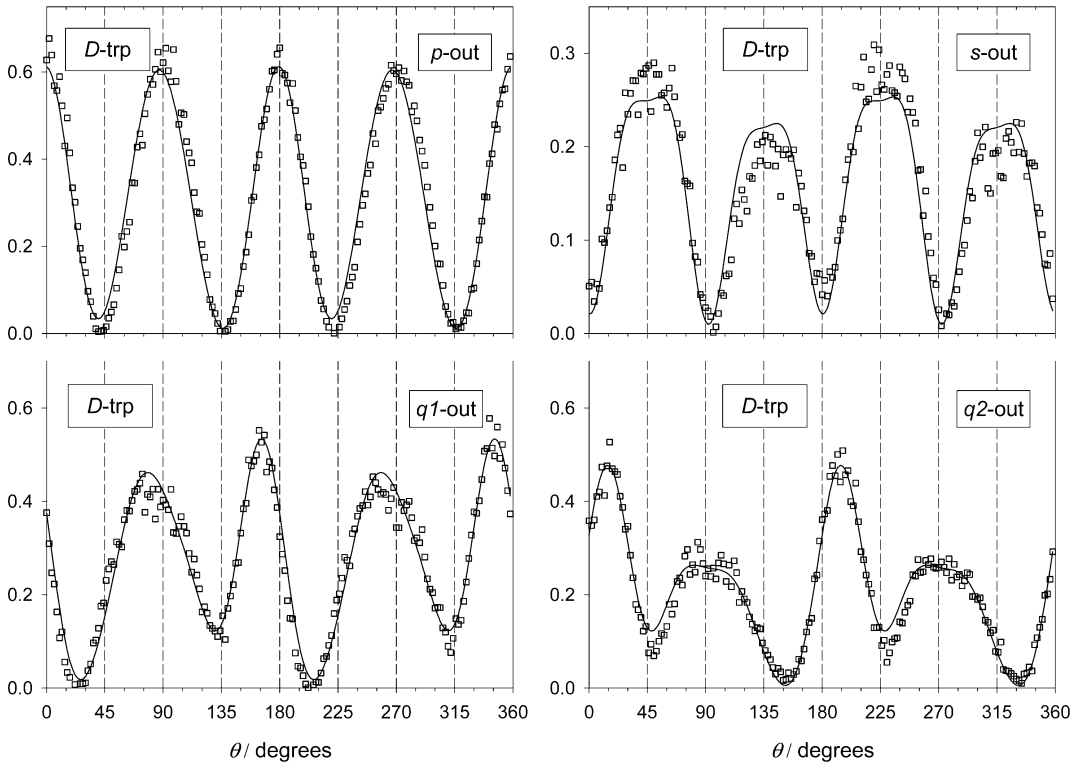

Figure 4. Global fits of wave plate rotation data $I_{2\omega}(\theta)$ for D-trp at the air/water interface, for the indicated polarization states of second harmonic radiation. ($q1$ and $q2$ represent q_{45} and q_{135} polarization states, respectively.) The wavelength of fundamental radiation was $\lambda = 564$ nm. The second harmonic intensity is shown in the same arbitrary units in all traces.

the magnitude of the sum of the squares of the deviations between measured and fitted traces. The correction was applied to all of our results and is included in Figures 3−6 and also in Table 1.

No attempt has been made to correct the measurements for the presence of a small background SHG signal that was observed for the buffer solution with no added tryptophan derivative or DHN. The associated error should be small, since the background signal was approximately 10-fold weaker than the working signals (Figure 2). The effective susceptibilities in Table 1 have been uniformly scaled by a normalization constant that was obtained from measurement of R_{pp} for z-quartz (section 3.1). For completeness, we also show in Table 1 the elements of the nonlinear susceptibility tensors, as absolute values in units of 10^{-22} m^2/V. The detailed expressions that relate the effective susceptibilities to the elements of the nonlinear susceptibility tensor have been given by Maki et al.[19] We assumed that the index of refraction of the monolayer film was the same as that of air, for both the fundamental and second harmonic frequencies. It is difficult to assess the uncertainties present in the results in Table 1. From repeated measurements on several of the trp systems, it was seen the results were subject to significant variability, but the main features were reproducible in the range ±30%.

In Figures 4 and 5, the *s*-out $I_{2\omega}(\theta)$ traces for D-trp and L-trp show well-defined asymmetry about $\theta = 180°$. This asymmetry shows a mirror-image relation for D-trp and L-trp enantiomers, as expected for chiral isotropic surfaces. Similar results were obtained for LL-trp and DD-trp, as shown in Figure 6. In contrast, no asymmetry appears in the *s*-out trace for the achiral system DHN (Figure 3), as expected. These observations indicate that the assumption of in-plane isotropy of the surfaces is justified.

Chiral asymmetry is generally less apparent in the *p*-out $I_{2\omega}(\theta)$ traces for the trp systems compared with the *s*-out traces. An exception is LL-trp, but here the enantiomer DD-trp appears not to show the corresponding mirror-image asymmetry (Figure 6). Thus, by using eqs 3 and 4 to fit the individual *p*-out traces, it was seen that the chiral parameters (h_{p1} and h_{p2}) did not show the expected sign change for enantiomers. However, by inclusion of the correction for the artifact in the fit, the parameters were brought closer to the expected relation. The correction had a much smaller effect on the fitted parameters for individual *s*-out traces, and thus, the chiral component of the *p*-out data is more sensitive to the distorting effect of the artifact.

It is useful to consider circular difference (CD) and linear difference (LD) effects in SHG from chiral surfaces.[29] These are second harmonic intensity differences for left-hand and right-hand circularly polarized fundamental radiation (CD) and for q_{45}- and q_{135}-polarized fundamental radiation (LD). The plane-polarized states q_{45} and q_{135} have been defined in section 3.2. Expressions for the normalized intensity differences in terms of effective susceptibilities of the chiral surface are shown in eqs 12 and 13.[29]

$$\Delta I_{\mathrm{CD}} = \frac{4[(f_2 - g_2)h_1 - (f_1 - g_1)h_2]}{f_1^2 + f_2^2 + g_1^2 + g_2^2 + h_1^2 + h_2^2 - 2(f_1g_1 + f_2g_2)} \tag{12}$$

$$\Delta I_{\mathrm{LD}} = \frac{-4[(f_1 + g_1)h_1 + (f_2 + g_2)h_2]}{f_1^2 + f_2^2 + g_1^2 + g_2^2 + h_1^2 + h_2^2 + 2(f_1g_1 + f_2g_2)} \tag{13}$$

The intensity differences are normalized to the average second harmonic intensity for the two polarization states of the fundamental. We calculated these quantities from the effective susceptibilities for the trp systems in Table 1, and the results are given in Table 2. ΔI_{CD} and ΔI_{LD} are given for both *s*- and *p*-polarized second harmonic radiation.

One expects to find a sign change in the intensity differences for the enantiomeric pairs (D-trp, L-trp) and (DD-trp, LL-trp), with

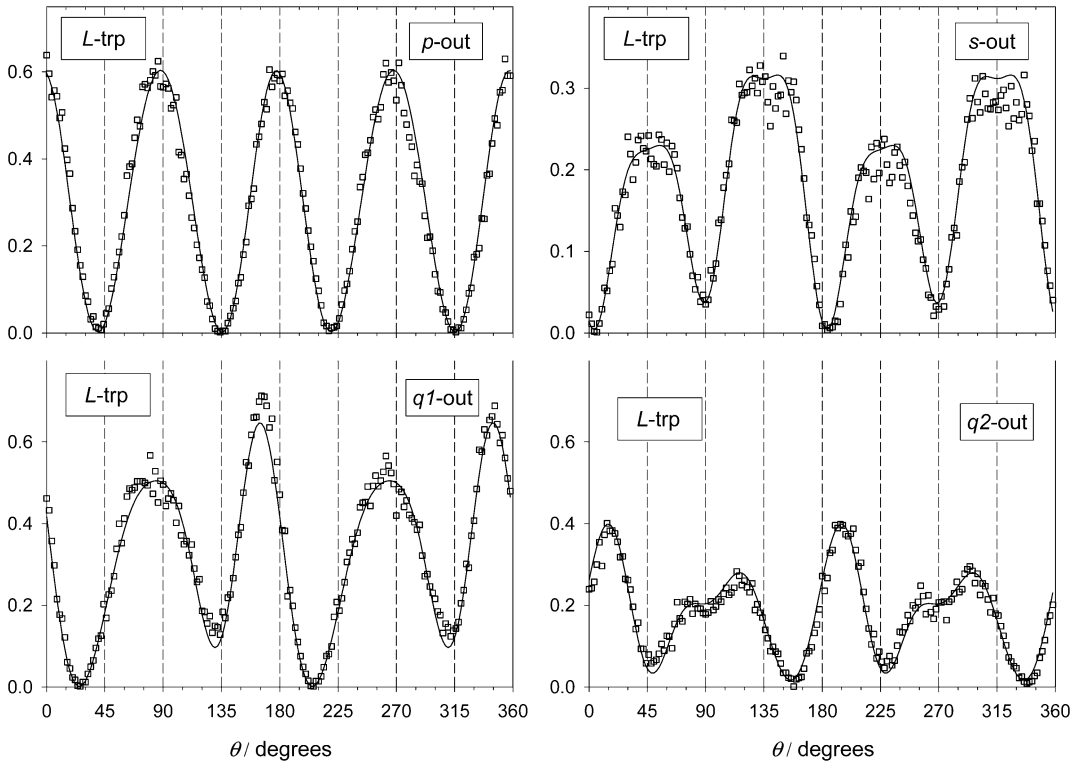

Figure 5. Global fits of wave plate rotation data $I_{2\omega}(\theta)$ for L-trp at the air/water interface, for the indicated polarization states of second harmonic radiation. ($q1$ and $q2$ represent q_{45} and q_{135} polarization states, respectively.) The wavelength of fundamental radiation was $\lambda = 564$ nm. The second harmonic intensity is shown in the same arbitrary units in all traces.

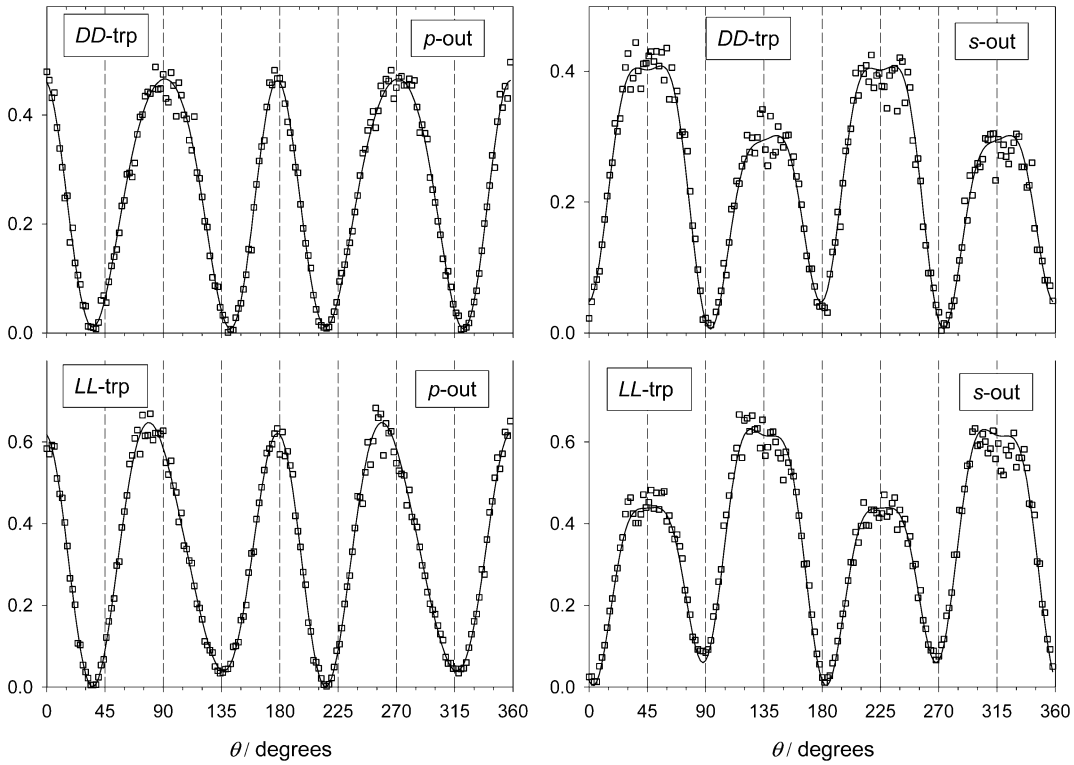

Figure 6. Fits of single traces of wave plate rotation data $I_{2\omega}(\theta)$ for DD-trp and LL-trp at the air/water interface, for the indicated polarization states of second harmonic radiation. The wavelength of fundamental radiation was $\lambda = 564$ nm. The second harmonic intensity is shown in the same arbitrary units in all traces.

the absolute magnitudes of the intensity differences preserved. A sign change is observed for most cases in Table 2, with the exception of ΔI_{LD} (*s*-out) for (D-trp, L-trp). However, the absolute magnitudes of the intensity differences are generally not in close agreement within the enantiomeric pairs. Exceptions are the *p*-out intensity differences ΔI_{CD} and ΔI_{LD} for (DD-trp, LL-trp), which show approximately conserved magnitudes and the expected sign changes. A further consistent feature of the results was noted when ΔI_{CD} (*s*-out) was evaluated from effective susceptibilities obtained by fitting single $I_{2\omega}(\theta)$ traces.

TABLE 2: Circular and Linear Differences of Second Harmonic Intensity for Several Tryptophan Derivatives Adsorbed at the Air/Water Interface, from Global Fits of Quarter-Wave Plate Rotation Data for $\lambda = 564$ nm[a]

	D-trp	L-trp	DD-trp	LL-trp
s-out				
ΔI_{CD}	−0.13	0.35	−0.18	0.22
ΔI_{LD}	0.086	0.077	−0.035	0.17
p-out				
ΔI_{CD}	−0.33	1.3	−0.38	0.36
ΔI_{LD}	0.023	−0.18	0.14	−0.16

[a] Intensity differences for *s*- and *p*-polarized components of second harmonic radiation. See the text for details.

TABLE 3: Circular Differences of Second Harmonic Intensity for L-trp and LL-trp Adsorbed at the Air/Water Interface, from Fits of Single Traces of Quarter-Wave Plate Rotation Data for Several Fundamental Wavelengths[a]

	wavelength/nm			
	542	564	581	603
L-trp: ΔI_{CD} (*s*-out)	0.45	0.41	0.49	0.09
LL-trp: ΔI_{CD} (*s*-out)	0.38	0.41	0.33	0.01

[a] Intensity differences for *s*-polarized component of second harmonic radiation. See the text for details.

These effective susceptibilities are distinct from those obtained from the global fits. Being associated with single *s*-out traces, they are not subject to the distorting effect of the artifact that affects mainly the *p*-out traces (see above). The ΔI_{CD} (*s*-out) evaluated from single traces are −0.33 (D-trp), 0.37 (L-trp), −0.33 (DD-trp), and 0.32 (LL-trp), which show enantiomeric effects as expected for isotropic chiral surfaces. Such measurements of ΔI_{CD} (*s*-out) are robust because the signal is relatively large and slowly varying in the region of the circular polarization states of the fundamental ($\theta = 45, 135°, ...$). The situation is much less favorable for the same measurements on *p*-out traces, since the *p*-out signal intensities are close to zero and quickly varying in these regions, as shown in Figure 5, for example. For similar reasons, it is difficult to make accurate measurements of ΔI_{LD} on single *s*-out or *p*-out $I_{2\omega}(\theta)$ traces. Except for ΔI_{CD} (*s*-out), our most reliable measurements of the intensity differences are from the global fits (Table 2). Our preferred measurements of ΔI_{CD} (*s*-out) are from the fits to single $I_{2\omega}(\theta)$ traces.

We measured ΔI_{CD} *s*-out intensity differences for L-trp and LL-trp for several fundamental wavelengths in the range 542−603 nm, by using effective susceptibilities obtained from fits of single *s*-out $I_{2\omega}(\theta)$ traces. The results are summarized in Table 3, which incorporates minor corrections for the artifact in the achromatic wave plate. L-trp and LL-trp show comparable values of ΔI_{CD} (*s*-out) in this range. In both cases there is little variation with fundamental wavelength except for an abrupt drop in ΔI_{CD} (*s*-out) at the longest wavelength (603 nm).

In general, our results show a close similarity between Boc-trp and Boc-trp-trp. Let us emphasize that the bulk solutions that were used were well characterized with respect to chemical composition. Despite the similarities, there are certain features of the SHG-OA results that allow a clear distinction to be made between Boc-trp and Boc-trp-trp. These features are apparent in the $I_{2\omega}(\theta)$ traces (Figures 4−6) and also in the details of the effective susceptibilities in Table 1. We found that the $I_{2\omega}(\theta)$ traces for L-trp did not vary with the concentration of the bulk solution, in a range where the surface density of L-trp changed by a factor ∼2. This suggests that the $I_{2\omega}(\theta)$ traces were not affected by interactions between the L-trp molecules.

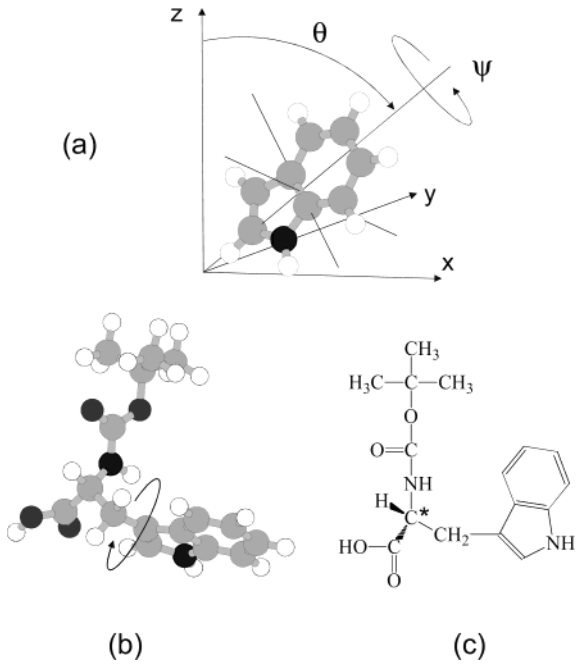

Figure 7. (a) Tilt (θ) and twist (ψ) angles of indole (C_8NH_7) relative to laboratory coordinate axes, with Z the normal to the air/water interface. The dark circle represents the nitrogen atom of indole. (b) Hypothetical structure of Boc-D-trp at the air/water interface, viewed from the $+Z$ direction. Note that the indicated bond torsion is correlated with the twist angle ψ. (c) Chemical structure of Boc-D-trp. The asymmetric carbon center is marked with an asterisk.

4. Discussion

In the following we consider the implications of our results for the interpretation of the SHG-OA effects in terms of a microscopic model. Our central result is a close similarity in SHG-OA for the like enantiomers L-trp and LL-trp on one hand and D-trp and DD-trp on the other. The presence of two trp residues in the dipeptide has only a small effect on the observed SHG-OA.

As shown in Figure 2, there is a correspondence between the absorption spectrum of Boc-trp in solution and the second harmonic spectrum of the air/solution interface. This indicates that the nonlinear response with the fundamental wavelength $\lambda \sim 560$ nm is resonantly enhanced at the two-photon level. The resonance is associated with the indole chromophore of tryptophan, with well-known electronic transitions to ^1L_a and ^1L_b excited states in the region near 280 nm.[32] The structure of indole is shown in Figure 7. The ^1L_a and ^1L_b excitations can be described as transitions within a planar π-electron system and are thus polarized in the plane of the indole molecule. This is a significant point when considering the origin of SHG-OA of the trp systems. A planar chromophore is of course achiral. However, the proximity of the chromophore to the asymmetric carbon of tryptophan means that the chromophore is in a chiral environment.

Our successful analysis of all $I_{2\omega}(\theta)$ traces strictly in terms of an electric-dipole model, with $g_s = 0$ and $h_p \propto f_s$, suggests that magnetic effects are not important for the trp systems. Recently, attention has been drawn to possible structural origins of SHG-OA,[26,27] within the framework of electric-dipole interactions. Note that an unambiguous analysis of SHG-OA relies on azimuthal isotropy of the surface (i.e., the surface must be rotationally invariant) or the rotational symmetry of the surface must be explicitly considered.[33] For an isotropic surface, asymmetry in the twist-angle (ψ) distribution of an achiral

chromophore about its polar axis may impart chirality to the surface and, thereby, give rise to SHG-OA. The polar axis defines the tilt angle (θ) of the chromophore relative to the surface normal. The tilt (θ) and twist (ψ) angles are illustrated in Figure 7 for the case of an indole chromophore. Simpson and co-workers[26,27] have suggested that asymmetry in the twist-angle distribution of an achiral chromophore could arise from the presence of a chiral center in the molecule. The chromophore may be sufficiently removed from the chiral center that no direct electronic coupling occurs, and the chromophore remains effectively achiral. The chiral center has the effect of directing assembly of the chromophore at the surface. Such an effect could be important for the trp systems studied in this work, but we believe that this is unlikely. To illustrate how the effect could operate, consider the model structure for Boc-trp at the air/water interface shown in Figure 7b. Note that the twist angle of the indole chromophore is related to the torsion angle indicated in Figure 7b. In particular, asymmetry in the twist angle distribution implies restricted rotation with respect to the torsion. Such a restricted rotation is unlikely considering the probable magnitude of the torsional barrier.[34] One could argue that intermolecular interactions in the surface layer might effectively lock the conformation, but this seems unlikely in view of the fluid nature of the air/water interface.

The above considerations lead to the suggestion that the origin of SHG-OA for the trp systems is an intrinsic molecular chiral response. Of course, Boc-trp and Boc-trp-trp are chiral molecules, but the asymmetric carbon centers are separated from the indole chromophores by a methylene ($-CH_2-$) linking group (see illustration in Figure 7). These compounds nevertheless display strong circular dichroism (CD) in linear spectroscopy in the spectral region below 230 nm[35] and generally much weaker CD effects in the region of the ^1L_a and ^1L_b excitations of indole near 280 nm.[36] These CD effects in linear spectroscopy of tryptophanyl compounds have their origin in dipole−dipole coupling between similar or dissimilar chromophores including indole and amide groups that are present in a chiral arrangement. The excited electronic states and associated intramolecular interactions that are responsible for strong circular dichroic effects in linear spectroscopy of tryptophan residues should also be significant for SHG-OA.

A coupled chromophore, electric-dipole mechanism of SHG-OA is potentially important for the dipeptide Boc-trp-trp, due to the presence of indole chromophores in spatial proximity. In the work of Frey and co-workers,[7] significant SHG-OA was observed for Boc-trp-trp at air/water interface but not for Boc-trp. These observations are suggestive of coupling between trp residues. However, in this study we found closely similar SHG-OA for Boc-trp and Boc-trp-trp, in disagreement with the report of Frey and co-workers. The origin of this discrepancy is not clear. Our observations indicate that excitonic coupling between indole chromophores is not a dominant mechanism of SHG-OA for Boc-trp-trp. Instead, the proximity of indole to an asymmetric carbon center may be the significant factor, as in the case of optical activity in linear spectroscopy. We believe that coupling between transition dipoles on indole and amide (NHCO) chromophores could give rise to the observed SHG-OA effects. These dissimilar chromophores are present in a chiral arrangement (see the chemical structure of Boc-trp in Figure 7). Such a mechanism for SHG-OA, involving coupling of dissimilar chromophores, is a generalization of the mechanism discussed by Hache et al.[24] and by Belkin et al.,[25] involving the coupling of two identical chromophores. The relative unimportance of interactions between indole chromophores in the dipeptide Boc-trp-trp can be understood by considering that the indole groups may be too far apart to allow significant coupling. We found no indication of SHG-OA for the peptide gramicidin, which includes several trp residues. This shows that the presence of trp is not a sufficient condition for observation of SHG-OA. The conformation and orientation of the peptide at the interface are additional important factors. In future work it is planned to continue this investigation of the origin of SHG-OA in these biomolecular/surface systems.

5. Conclusion

We have measured the second-order nonlinear susceptibility tensors for monolayer films of two enantiomerically pure tryptophan derivatives and for an achiral hydroxynaphthyl derivative at the air/water interface, for the fundamental wavelength $\lambda = 564$ nm. A satisfactory analysis of data from quarter-wave plate rotation measurements was obtained by using the assumption that only electric-dipole effects contributed to the nonlinear response. Optical isomers of mono- and ditryptophan compounds show approximately equal magnitudes and opposite signs of the chiral components of the nonlinear susceptibilities, as expected for isotropic surface films. Spectra of the second harmonic efficiency versus fundamental wavelength for the tryptophan derivatives showed resonance enhancement at the two-photon level, associated with the indole chromophore of tryptophan. An interpretation of our results in terms of an asymmetric orientational distribution of the (achiral) indole chromophore appears not to be applicable. Instead, it is suggested that the nonlinear chiral response may have its origin in dipole coupling between chromophores, as in the case of circular dichroism in linear spectroscopy of tryptophan derivatives. From a practical point of view, it is significant that the nonlinear response is observed in a lower energy spectral region ($\lambda/2 \sim 280$ nm) compared with the strongest chiral effects in linear spectroscopy ($\lambda < 230$ nm). From a comparison of results for mono- and ditryptophan derivatives, no evidence was found for excitonic coupling effects in the nonlinear chiral response. The peptide gramicidin showed no detectable optical activity in second harmonic reflection from the air/water interface. This shows that the presence of one or more tryptophan residues in a peptide or protein is not a sufficient condition for observation of optical activity in second harmonic reflection.

Acknowledgment. The authors thanks Prabhat Arya and Michael Barnes for chemical synthesis of Boc-trp-trp and Linda Johnston for assistance in the work on gramicidin D.

References and Notes

(1) Petralli-Mallow, T.; Wong, T. M.; Byers, J. D.; Yee, H. I.; Hicks, J. M. *J. Phys. Chem.* **1993**, *97*, 1383.
(2) Byers, J. D.; Yee, H. I.; Hicks, J. M. *J. Chem. Phys.* **1994**, *101*, 6233.
(3) Byers, J. D.; Yee, H. I.; Petralli-Mallow, T.; Hicks, J. M. *Phys. Rev. B* **1994**, *49*, 14643.
(4) Kauranen, M.; Verbiest, T.; Maki, J. J.; Persoons, A. *J. Chem. Phys.* **1994**, *101*, 8193.
(5) Verbiest, T.; Kauranen, M.; Persoons, A.; Ikonen, M.; Kurkela, J.; Lemmetyinen, H. *J. Am. Chem. Soc.* **1994**, *116*, 9203.
(6) Stolle, R.; Loddoch, M.; Marowsky, G. *Nonlinear Opt.* **1994**, *8*, 79.
(7) Crawford, M. J.; Haslam, S.; Probert, J. M.; Gruzdkov, Y. A.; Frey, J. G. *Chem. Phys. Lett.* **1994**, *229*, 260.
(8) Fasman, G. D., Ed.; *Circular dichroism and the conformational analysis of biomolecules*; Plenum Press: New York, 1996.
(9) Shen, Y. R. *Annu. Rev. Phys. Chem.* **1989**, *40*, 327.
(10) Smiley, B. L.; Vogel, V. *J. Chem. Phys.* **1995**, *103*, 3140.
(11) Vogel, V.; Smiley, B. L. *Proc. SPIE* **1992**, *1922*, 86.
(12) Smiley, B. L.; Vogel, V. *Proc. SPIE* **1994**, *2125*, 59.

(13) Petralli-Mallow, T. P.; Plant, A. L.; Lewis, M. L.; Hicks, J. M. *Langmuir* **2000**, *16*, 5960.
(14) Kriech, M. A.; Conboy, J. C. *J. Am. Chem. Soc.* **2003**, *125*, 1148.
(15) (a) Rinuy, J.; Brevet, P. F.; Girault, H. H. *Biophys. J.* **1999**, *77*, 3350. (b) Perrenoud-Rinuy, J.; Brevet, P. F.; Girault, H. H. *Phys. Chem. Chem. Phys.* **2002**, *4*, 4774.
(16) Watry, M. R.; Richmond, G. L. *J. Phys. Chem. B* **2002**, *106*, 12517.
(17) Kim, G. K.; Gurau, M. C.; Lim, S. M.; Cremer, P. S. *J. Phys. Chem. B* **2003**, *107*, 1403.
(18) (a) Wang, J.; Clarke, M. L.; Zhang, Y.; Chen, X.; Chen, Z. *Langmuir* **2003**, *19*, 7862. (b) Wang, J.; Buck, S. M.; Even, M. A.; Chen, Z. *J. Am. Chem. Soc.* **2002**, *124*, 13302. (c) Wang, J.; Buck, S. M.; Chen, Z. *J. Phys. Chem. B* **2002**, *106*, 11666.
(19) Maki, J. J.; Kauranen, M.; Persoons, A. *Phys. Rev. B* **1995**, *51*, 1425.
(20) Kauranen, M.; Verbiest, T.; Persoons, A. *J. Mod. Opt.* **1998**, *45*, 403.
(21) Hache, F.; Mesnil, H.; Schanne-Klein, M. C. *J. Chem. Phys.* **2001**, *115*, 6707.
(22) Schanne-Klein, M. C.; Hache, F.; Brotin, T.; Andraud, C.; Collet, A. *Chem. Phys. Lett.* **2001**, *338*, 159.
(23) Schanne-Klein, M. C.; Boulesteix, T.; Hache, F.; Alexandre, M.; Lemercier, G.; Andraud, C. *Chem. Phys. Lett.* **2002**, *362*, 103.
(24) Hache, F.; Boulesteix, T.; Schanne-Klein, M. C.; Alexandre, M.; Lemercier, G.; Andraud, C. *J. Phys. Chem. B* **2003**, *107*, 5261.
(25) Belkin, M. A.; Shen. Y. R.; Flytzanis, C. *Chem. Phys. Lett.* **2002**, *363*, 479.
(26) Simpson, G. J. *J. Chem. Phys.* **2002**, *117*, 3398.
(27) Simpson, G. J.; Perry, J. M.; Ashmore-Good, C. L. *Phys. Rev. B* **2002**, *66*, 165437.
(28) Geiger, F.; Stolle, R.; Marowsky, G.; Palenberg, M.; Felderhof, B. U. *Appl. Phys. B* **1995**, *61*, 135.
(29) Maki, J. J.; Verbiest, T.; Kauranen, M.; Van Elshocht, S.; Persoons, A. *J. Chem. Phys.* **1996**, *105*, 767.
(30) Maki, J. J.; Kauranen, M.; Verbiest, T.; Persoons, A. *Phys. Rev. B* **1997**, *55*, 5021.
(31) Roberts, D. A. *IEEE J. Quantum Electron.* **1992**, *28*, 2057.
(32) Callis, P. R. *J. Chem. Phys.* **1991**, *95*, 4230.
(33) Verbiest, T.; Kauranen, M.; Van Rompaey, Y.; Persoons, A. *Phys. Rev. Lett.* **1996**, *77*, 1456.
(34) Electronic structure calculations on Boc-trp using the semiempirical AM1 Hamiltonian indicated that the torsional barrier was less that 2 kcal/mol, for a range of model geometries.
(35) Auer, H. E. *J. Am. Chem. Soc.* **1973**, *95*, 3003.
(36) Strickland. E. H. *CRC Crit. Rev. Biochem.* **1974**, *2*, 113.